Syntheses, Characterization, and Computational Study of AsF_5 Adducts with Ketones

Daniel Stuart[a,b], Stacey D. Wetmore[a,b], and Michael Gerken[*a,b]

[a]Canadian Centre for Research in Advanced Fluorine Technologies and [b]Department of Chemistry and Biochemistry, University of Lethbridge, 4401 University Drive W, Lethbridge, AB, CA T1K 3M4

[*]Corresponding author. Tel.: +1-403-329-2173; Fax: +1-403-329-2057; E-mail address: michael.gerken@uleth.ca.

Congratulations to Norio Shibata on receiving the 2019 ACS Award for Creative Work in Fluorine Chemistry

Abstract

Lewis acid-base adducts between AsF_5 and the ketones, acetone, cyclopentanone, and adamantanone, were synthesized from SO_2 and CH_2Cl_2 solutions. These adducts, which contain O---As pnictogen bonding interactions, were found to be stable in solutions at room temperature. Raman and NMR spectroscopy of the solid adducts showed a characteristic decrease in the C=O stretching frequency, as well as dramatic deshielding of the ^{13}C resonance of the carbonyl group upon adduct formation. Fluorine-19 NMR spectroscopy showed the two fluorine environments of the O−AsF_5 moiety. Optimization of the gas-phase geometry using DFT calculations yielded geometries with essentially planar CC=OAs moieties. NBO analyses of the adducts and the free ketones show the polarization of the C=O bond upon adduct formation. The lowering of the LUMO energies upon adduct formation is more dramatic than what was found for protonation of ketones and reflects the substantially enhanced electrophilicity of the adducted ketones.

Keywords:

Lewis-acid-base adducts; Pnictogen bonding; Ketones; Raman spectroscopy; DFT calculations

1. Introduction

Lewis acids are commonly used in a variety of organic chemistry reactions including Friedel-Crafts, aldol, and Diels-Alder reactions. Our interest in Lewis acid-base adducts of ketones with strong Lewis acids stems from the report that Lewis acids catalyse deoxofluorination of ketones by SF_4 [1] and our continuing interest in species present in such deoxofluorination reactions [2]. Lewis acid reagents commonly used in organic chemistry include the readily available $AlCl_3$, $TiCl_4$, BF_3, and $SnCl_4$. The mechanism involves the binding of the Lewis acid to a Lewis basic substrate, frequently a ketone or aldehyde, which is accompanied by withdrawal of electron density

from the functional group, such as the C=O group. This lowers the energy of the LUMO, making the carbonyl carbon center more readily accessible for nucleophilic attack [3].

Early infrared spectroscopic studies of the $AlCl_3 \cdot O{=}CCl_2$ adduct showed a decrease of 173 cm^{-1} in the C=O stretching frequency upon adduct formation, which is indicative of an oxygen-bridged coordination complex as opposed to the formation of the ionic structure $[ClCO][AlCl_4]$ [4]. The relatively low Lewis basicity of neutral, organic oxygen bases results in low stability of the adducts. In the case of $AlCl_3 \cdot O{=}CCl_2$, full dissociation occurred under ambient conditions [4,5]. A number of X-ray crystallographic studies have been carried out on main-group Lewis acid-base adducts with carbonyl compounds [6,7]. The crystal structure of the $BF_3 \cdot$benzaldehyde adduct shows a B---O interaction of 1.59 Å with an *E*-configuration about the carbonyl moiety [3]. Semi-empirical MNDO (Modified Neglect of Diatomic Overlap) calculations of the $BF_3 \cdot O{=}CHCH_3$ adduct showed the *E*-configuration to be more favourable over the *Z*-configuration by 7.5 kJ/mol [3]. The *E*-configuration was also calculated to be lower than the *Z*-configuration for protonated benzaldehyde and acetaldehyde [2]. A ^{13}C NMR spectroscopic study of Lewis acid-base adducts between BF_3 and various aliphatic ketones, such as acetone and cyclopentanone, showed the ^{13}C resonances of the carbonyl carbons to shift to higher frequencies by 24.3 and 26.2 ppm, respectively [8]. A crystallographic study of 1:1 $AlCl_3 \cdot$tetramethylurea showed the presence of an Al---O interaction with an Al–O distance of 1.78 Å and an Al–O–C angle of 132.5° [9]. Laube et al. have prepared adducts of ketones with $SbCl_5$, which were structurally characterized by X-ray crystallography [7].

Employing the strong Lewis acids AsF_5 and SbF_5, Chen and Passmore were able to synthesize the 1:1 adduct of $O{=}CF_2$ [10]. Low-temperature Raman spectroscopy in both the liquid and solid states showed a decrease by 118 (liquid: 67) and 136 (liquid: 99) cm^{-1} in the C=O

stretching frequency upon formation of the oxygen-bridged adducts $AsF_5 \cdot O{=}CF_2$ and $SbF_5 \cdot O{=}CF_2$, respectively, compared to free $O{=}CF_2$. Dissociation occurred upon warming to RT, however, the reactions were found to be reversible in all cases. Christe and co-workers synthesized the 1:1 adducts of $O{=}CCl_2$, $O{=}CClF$, and $O{=}CF_2$ with AsF_5 and SbF_5, and also found them to dissociate at ambient temperature [5]. Vibrational and multinuclear NMR spectroscopies were used to characterize these Lewis acid-base adducts at low temperatures. Upon adduct formation, the ν(CO) stretching frequencies significantly decreased by upwards of 240 cm^{-1} ($O{=}CCl_2$), 199 cm^{-1} ($O{=}CClF$) and 158 cm^{-1} ($O{=}CF_2$). Geometries were optimized in the gas phase at the B3LYP/SBK+(d) level of theory and the calculated energies were used to determine the relative stability amongst the carbonyl halide adducts with AsF_5 and SbF_5, with $SbF_5 \cdot O{=}CCl_2$ being the most stable towards dissociation. While these adducts with carbonyl halides were oxygen-bridged, Sb_3F_{15} was found to be Lewis acidic enough towards $O{=}CClF$ to yield the $[OCCl][Sb_3F_{16}]$ salt [11].

A matrix-isolation study has shown a range of ketones, including acetone, cyclopentanone, and adamantanone, to form complexes with SbF_5. Vibrational spectroscopy, complemented with semi-empirical and *ab initio* calculations, showed decreases in the characteristic C=O stretching frequencies [12].

The current study targets the isolation of bulk quantities of AsF_5 adducts with the aliphatic ketone acetone, the monocyclic ketone cyclopentanone, and the bulky polycyclic ketone 2-adamantanone, together with their Raman and multi-nuclear NMR spectroscopic characterization and density functional theory (DFT) calculations.

2. Results and Discussion

2.1. Synthesis and Properties of Lewis Acid-Base Adducts of Acetone, Cyclopentanone, and 2-Adamantanone with AsF_5

Three ketones, i.e., acetone ($O=C(CH_3)_2$), cyclopentanone ($O=C_5H_8$), and 2-adamantanone ($O=C_{10}H_{14}$), which are aliphatic, monocyclic and polycyclic, respectively, in nature, were chosen for reactions with stoichiometric amounts of AsF_5 in SO_2. The reactions were allowed to proceed at −78 °C. Dichloromethane was also a suitable solvent for reactions with 2-adamantanone and cyclopentanone. Using CH_2Cl_2 resulted in instantaneous reactions forming insoluble fine, white powders, whereas using SO_2 resulted in clear, colourless solutions. Removing the solvent at −78 °C yielded white powders identified by low-temperature (LT) Raman spectroscopy as the 1:1 adducts of $AsF_5 \cdot O=R$ (where R = $C(CH_3)_2$, C_5H_8, or $C_{10}H_{14}$). Single crystal growth of these adducts from SO_2 and CH_2Cl_2 was attempted but was unsuccessful.

$$O=R + AsF_5 \xrightarrow{SO_2 \text{ or } CH_2Cl_2} AsF_5 \cdot O=R \quad (R = C(CH_3)_2, C_5H_8, C_{10}H_{14}) \qquad (1)$$

These adducts were characterized in solution by ^1H, ^{13}C, and ^{19}F NMR spectroscopy in SO_2 and were found to be stable at room temperature (RT), even after 40 min. A colour change was observed for the $AsF_5 \cdot O=C(CH_3)_2$ adduct in SO_2 to yellow, possibly as a result of some acetone undergoing oxidation due to the presence of excess AsF_5 in solution. Solutions of $AsF_5 \cdot O=C_5H_8$, and $AsF_5 \cdot O=C_{10}H_{14}$ were stable in SO_2 and did not show any colour change upon warming to RT. Solid samples did not exhibit such stability. Upon warming the sample of solid $AsF_5 \cdot O=C(CH_3)_2$ to RT, it quickly decomposed into a dark yellow powder unidentifiable by Raman spectroscopy due to significant fluorescence. The $AsF_5 \cdot O=C_5H_8$ and $AsF_5 \cdot O=C_{10}H_{14}$ adducts were stable at RT for roughly 1 h before the samples began turning light brown in colour. While LT Raman spectroscopy showed fluorescence in the baseline, the most intense Raman bands attributable to the adducts were still observed. After two days at RT the $AsF_5 \cdot O=C_5H_8$ and $AsF_5 \cdot O=C_{10}H_{14}$

adducts had turned into grey powders with no discernible signals in the Raman spectra due to a large fluorescence.

2.2. Raman Spectroscopy

The Raman spectra of solid $AsF_5{\cdot}O{=}C(CH_3)_2$, $AsF_5{\cdot}O{=}C_5H_8$, and $AsF_5{\cdot}O{=}C_{10}H_{14}$ were recorded at −100 °C and are depicted in Fig. 1. Vibrational frequencies of the gas-phase geometry-optimized compounds were calculated and used to aid in the assignments of the Raman bands. The complete list of experimental and calculated vibrational bands can be found in Tables S1 to S3 (Supporting Information).

Table 1

Observed and calculated ν(CO) frequencies (cm^{-1}) for $AsF_5{\cdot}O{=}C(CH_3)_2$, $AsF_5{\cdot}O{=}C_5H_8$, and $AsF_5{\cdot}O{=}C_{10}H_{14}$, as well as their free ketones.

Compounds	exptl [a]	calcd [b]
$O{=}C(CH_3)_2$	1751(3) 1709(16)	1782(13)[195][c]
$AsF_5{\cdot}O{=}C(CH_3)_2$	1592(2)	1683(5)[344][c]
$SbF_5{\cdot}\ O{=}C(CH_3)_2$	1590 [d]	--
$O{=}C_5H_8$	1743(16) 1727(23)	1806(15)[264][c]
$AsF_5{\cdot}O{=}C_5H_8$	1620(6) 1604(2)	1706(4)[422][e]
$SbF_5{\cdot}O{=}C_5H_8$	1610 [d]	--
$O{=}C_{10}H_{14}$	1719(13)	1779(17)[280][c]
$AsF_5{\cdot}O{=}C_{10}H_{14}$	1577(6) 1568(9) 1553(3)	1668(7)[513][e]
$SbF_5{\cdot}O{=}C_{10}H_{14}$	1550 [d]	--

[a] Relative Raman intensities are given in parentheses. [b] Unscaled Raman intensities, in $Å^4\ u^{-1}$, are given in parentheses; infrared intensities, in km mol^{-1}, are given in square brackets. [c] DFT calculations at the B3LYP/aug-cc-pVTZ level of theory. [d] Matrix-isolation study from reference 12. [e] DFT calculations at the B3LYP/cc-pVTZ level of theory.

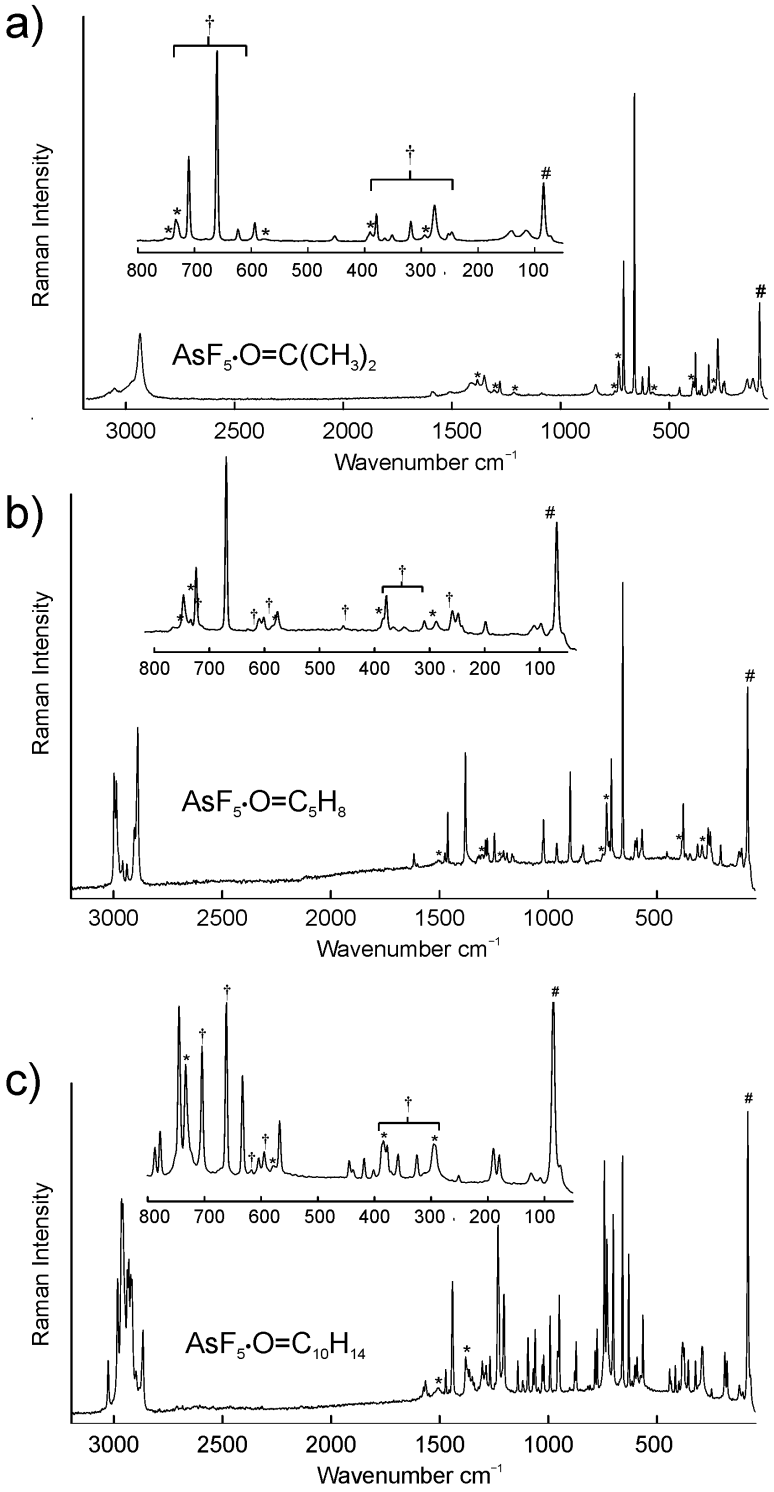

Fig. 1. Raman spectra of (a) $AsF_5{\cdot}O{=}C(CH_3)_2$ (b) $AsF_5{\cdot}O{=}C_5H_8$ and (c) $AsF_5{\cdot}O{=}C_{10}H_{14}$ at −100 °C. Symbols denote bands arising from FEP sample tube (*), an instrumental artifact (#), and the AsF_5 vibrations (†).

The interaction of the Lewis acid, AsF_5, with each ketone resulted in changes of vibrational bands associated with the ketone moieties in the Raman spectra. A comparison of the ν(CO) frequencies is found in Table 1. Formation of the $AsF_5{\cdot}O{=}C(CH_3)_2$ adduct caused a decrease in the C=O stretching frequency by 117 cm^{-1} compared to neat acetone. The $AsF_5{\cdot}O{=}C_5H_8$ and $AsF_5{\cdot}O{=}C_{10}H_{14}$ compounds showed decreases of 107 and 151 cm^{-1} relative to their parent ketones, respectively. A previous matrix-isolation study of the complementary SbF_5 adducts, $SbF_5{\cdot}O{=}C(CH_3)_2$ ($\Delta\nu$ = 110 cm^{-1}), $SbF_5{\cdot}O{=}C_5H_8$ ($\Delta\nu$ = 125 cm^{-1}), and $SbF_5{\cdot}O{=}C_{10}H_{14}$ ($\Delta\nu$ = 165 cm^{-1}), used infrared spectroscopy to show similar decreases in the C=O stretching frequencies [12]. The magnitudes of decreases in C=O stretching frequencies have been correlated to the number of $C_\alpha{-}C_\beta$ bonds, which is related to the degree a positive charge on the carbonyl carbon can be stabilized via inductive effects. These changes in frequencies are also comparable to salts of the monoprotonated ketones $[HO{=}C(CH_3)_2]^+$ ($\Delta\nu$ = 116 cm^{-1}), $[HO{=}C_5H_8]^+$ ($\Delta\nu$ = 122 cm^{-1}), and $[HO{=}C_{10}H_{14}]^+$ ($\Delta\nu$ = 155 cm^{-1}) [2]. Calculated frequencies of the geometry-optimized gas-phase structures predicted slightly smaller decreases in C=O frequencies ($AsF_5{\cdot}O{=}C(CH_3)_2$, 99 cm^{-1}; $AsF_5{\cdot}O{=}C_5H_8$, 100 cm^{-1}; and $AsF_5{\cdot}O{=}C_{10}H_{14}$, 111 cm^{-1}). The ν_s(CCC) stretching frequency of $AsF_5{\cdot}O{=}C(CH_3)_2$ (838 cm^{-1}) is found to be significantly higher than that of neat acetone (788 cm^{-1}). Comparable to similar trends for the monoprotonated ketones [2] and previously studied ketone-Lewis acid adducts [7], the interaction of AsF_5 with the carbonyl group causes a strengthening of the C−C(O) bonds.

The vibrational frequencies associated with the AsF_5 moiety in the adducts are listed in Table 2. The characteristic As−F stretches of adducted AsF_5 appear as intense bands in the Raman spectra. For $AsF_5{\cdot}O{=}C(CH_3)_2$, the $\nu_s(AsF_{4,eq})$ stretching frequency at 660 cm^{-1} was the most intense Raman band. The second most intense band at 710 cm^{-1} was assigned to the $\nu(AsF_{ax})$

stretching frequency. The frequencies of these bands are rather invariant between the adducts of the three ketones: $AsF_5 \cdot O{=}C_5H_8$ ($\nu(AsF_{ax})$ 711; $\nu_s(AsF_{4,eq})$ 659 cm^{-1}) and $AsF_5 \cdot O{=}C_{10}H_{14}$ ($\nu(AsF_{ax})$ 704; $\nu_s(AsF_{4,eq})$ 661 cm^{-1}). The calculated $\nu(AsF_{ax})$ stretches for the adducts were slightly overestimated (by upwards of 25 cm^{-1}) and $\nu_s(AsF_{4,eq})$ stretches were underestimated (by upwards of 9 cm^{-1}) when compared to the experimental values. The intense Raman band associated with the $\nu_s(AsF_{4,eq})$ and $\nu(AsF_{ax})$ modes appear at substantially lower frequencies compared to the AsF_5 adducts of the carbonyl halides, $COCl_2$, COClF, and COF_2 [5], which is likely the consequence of a higher Lewis basicity of the organic ketones in this study that donate more electron density towards the AsF_5 moiety. As expected, the degeneracy of the E-modes of free square-planar AsF_5 is removed in the adducts and most splitting into two components was observed in the low-temperature Raman spectra.

Table 2

Observed and calculated vibrational frequencies (cm^{-1}) for of the AsF_5 moiety in $AsF_5{\cdot}O{=}C(CH_3)_2$, $AsF_5{\cdot}O{=}C_5H_8$, and $AsF_5{\cdot}O{=}C_{10}H_{14}$. The symmetry species of the square pyramidal AsF_5 moiety are given in terms of the C_{4v} point group.

Approximate mode description[a]	$AsF_5{\cdot}O{=}C(CH_3)_2$ exptl[b]	$AsF_5{\cdot}O{=}C(CH_3)_2$ calcd[c]	$AsF_5{\cdot}O{=}C_5H_8$ explt[b]	$AsF_5{\cdot}O{=}C_5H_8$ calcd[c]	$AsF_5{\cdot}O{=}C_{10}H_{14}$ explt[b]	$AsF_5{\cdot}O{=}C_{10}H_{14}$ calcd[c]
$\nu_{as}(AsF_4, eq)$ (E)	729sh	729(1)[156]	704sh	739(1)[128]	733(65)	733(12)[114][f]
	679(1)	728(1)[154]		737(1)[144]	725sh	733(0)[139]
$\nu(AsF_{ax})$ (A_1)	710(44)	727(7)[163]	711(39)	735(6)[187]	704(75)	729(4)[177]
$\nu_s(AsF_{4,eq})$ (A_1)	660(100)	651(26)[9]	659(100)	655(23)[11]	661(100)	653(21)[14]
$\nu_{as}(AsF_{4,eq})$ (B_1)	623(6)	586(2)[2]	622(2)	594(2)[3]	617(4)	591(2)[2]
$\delta_{i.p.}(AsF_{4,eq})$ (E)	393sh	380(0)[46]	391sh	382(0)[44]	402(6)	384(0)[37]
	390(5)					
	364(2)	371(0)[30][d]	369(3)	374(0)[39]	371(5)	373(0)[48]
$\delta_{sciss}(AsF_{4,eq})$ (B_2)	379(20)	375(1)[11][e]	386sh	375(1)[5]	384(23)	373(1)[3]
			381(22)		377(20)	
$\delta(FAsF_4)$ (E)	318(11)	320(0)[0]	314(8)	321(1)[0]	325(15)	334(1)[0]
	277(20)	295(1)[0]	266(15)	296(1)[0]	295(22)	285(0)[0][g]
$\delta_{umbr}(AsF_{4,eq})$ (A_1)	351(4)	355(0)[148]	350(3)	360(0)[167]	358(15)	357(0)[187]
$\delta_{pucker}(AsF_{4,eq})$ (B_1)	n.o.	202(0)[0]	n.o.	204(0)[0]	n.o.	208(0)[0]

[a] The abbreviations denote symmetric (s), asymmetric (as), stretch (ν), bend (δ), scissoring (sciss), in-plane (i.p.), umbrella (umbrella), axial (ax), and equatorial (eq). The symmetry species of the modes of free square-planar AsF_5 (C_{4v} symmetry) is given in parentheses.[b] Relative Raman intensities are given in parentheses. The abbreviations denote shoulder (sh) and not observed (n.o.). [c] DFT calculations at the B3LYP/aug-cc-pVTZ level of theory. Unscaled Raman intensities, in $Å^4\ u^{-1}$, are given in parentheses; infrared intensities, in km mol^{-1}, are given in square brackets; DFT calculations at the B3LYP/cc-pVTZ level of theory. [d] More accurate mode description is $\delta_{sciss}(AsF_2)_{endo}$ (B_2/E). [e] More accurate mode description is $\delta_{sciss}(AsF_2)_{exo}$ (B_2/E). [f] Mode contains cage breathing motion. [g] Overlap with FEP mode and mode contains rocking motion of CH_2 groups.

2.3. NMR Spectroscopy

The ^{19}F, ^{13}C and ^{1}H NMR spectra of the adducts were recorded at 20 °C in liquid SO_2, as well as ^{19}F and ^{1}H NMR spectra at −70 °C. The NMR data of $AsF_5{\cdot}O{=}C(CH_3)_2$, $AsF_5{\cdot}O{=}C_5H_8$, and $AsF_5{\cdot}O{=}C_{10}H_{14}$ are listed in Table 3 and the ^{19}F NMR spectra are depicted in Figure 2.

At −70 °C, the ^{19}F NMR spectra of $AsF_5{\cdot}O{=}C(CH_3)_2$, $AsF_5{\cdot}O{=}C_5H_8$, and $AsF_5{\cdot}O{=}C_{10}H_{14}$ adducts contained two multiplets: doublets arising from the equatorial fluorine environments of AsF_5 and quintets arising from the axial fluorine atoms of AsF_5 with scalar $^2J(^{19}F{-}^{19}F)$ couplings of 124 or 125 Hz.

Table 3 ^{19}F, ^{1}H, and ^{13}C NMR parameters for $AsF_5{\cdot}O{=}C(CH_3)_2$, $AsF_5{\cdot}O{=}C_5H_8$, and $AsF_5{\cdot}O{=}C_{10}H_{14}$, as well as their neutral ketones, in SO_2 solvent.

	$O{=}C(CH_3)_2$	$AsF_5{\cdot}O{=}C(CH_3)_2$	
	20 °C	20 °C	−70 °C
$\delta(^{19}F)$ (ppm) [a],		−48.0 (s) {330}	−48.4 (d) {90} [b]
$\{\Delta\nu_{1/2}$ in Hz$\}$		−76.4 (s) {440}	−73.3 (qn) {105} [b]
$^2J(^{19}F{-}^{19}F)$ (Hz)			124
$\delta(^1H)$ (ppm)	2.77	3.34	3.05
$\delta(^{13}C)$ (ppm)	210.8 (CO)	238.5 (CO)	
	31.1 (α)	32.7 (qn, α); J = 2.3 Hz	
	$O{=}C_5H_8$	$AsF_5{\cdot}O{=}C_5H_8$	
$\delta(^{19}F)$ (ppm) [a],		−50.6 (s) {330}	−50.9 (d) {61}
$\{\Delta\nu_{1/2}$ in Hz$\}$		−76.3 (s) {450}	−73.3 (qn) {62}
$^2J(^{19}F{-}^{19}F)$ (Hz)			124
$\delta(^1H)$ (ppm)	2.72, 2.53	3.63	3.44, 3.34,
		2.78	2.50
$\delta(^{13}C)$ (ppm)	225.1 (CO)	252.1 (CO)	
	38.7 (α)	43.6 (qn,α) J = 2.0 Hz	
	23.7 (β)	24.0 (β)	
	$O{=}C_{10}H_{14}$	$AsF_5{\cdot}O{=}C_{10}H_{14}$	
$\delta(^{19}F)$ (ppm) [a],		−46.5 (s) {350}	−46.7 (d) {53}
$\{\Delta\nu_{1/2}$ in Hz$\}$		−74.5 (s) {450}	−71.6 (qn) {49}
$^2J(^{19}F{-}^{19}F)$ (Hz)			125
$\delta(^1H)$ (ppm)	3.14 (α)	3.87 (α)	3.29 (α)
	2.75, 2.72, 2.62, 2.56	3.03, 2.98, 2.86, 2.82 (β)	2.72, 2.68, 2.55, 2.51 (β)
		2.67 (γ)	2.36 (γ)
		2.31 (δ)	2.27 (δ)
$\delta(^{13}C)$ (ppm)	221.1 (CO)	250.0 (CO)	
	44.6 (α)	48.4 (α)	
	37.2 (β)	43.5 (β)	
	34.0 (γ)	36.1 (γ)	
	25.4 (δ)	27.8 (δ)	

[a] Abbreviations: (s) singlet; (d) doublet; (qn) quintet; (eq) equatorial; (ax) axial. [b] Obtained by spectral simulation using Mestre Nova

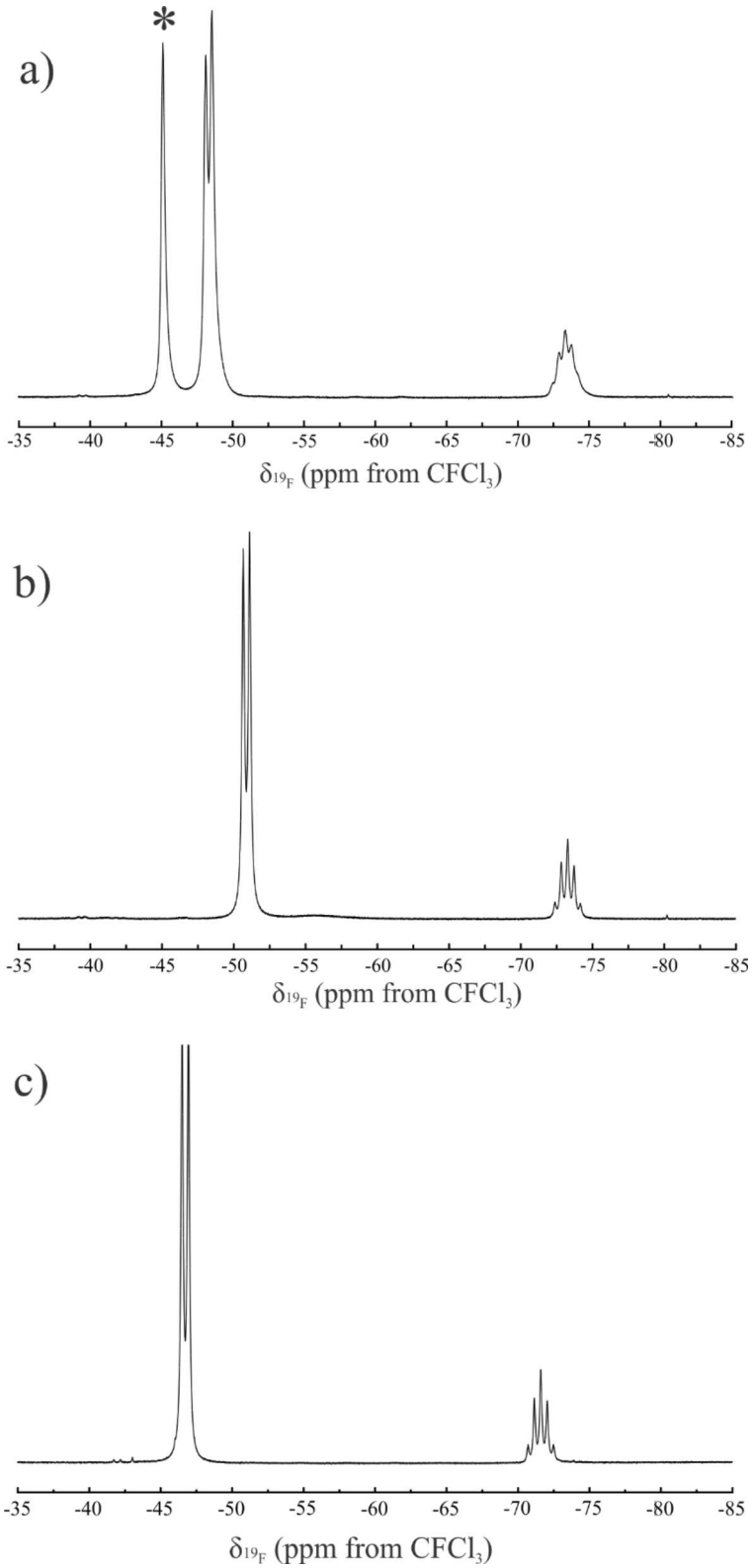

Fig. 2. ^{19}F NMR spectrum of (a) $AsF_5{\cdot}O{=}C(CH_3)_2$, (b) $AsF_5{\cdot}O{=}C_5H_8$, and (c) $AsF_5{\cdot}O{=}C_{10}H_{14}$ (c) adducts in liquid SO_2 at −70 °C. Externally referenced to $CFCl_3$. The symbol (*) denotes the $AsF_5{\cdot}SO_2$ signal.

The electric field gradient about ^{75}As in these adducts causes rapid quadrupolar relaxation of the ^{75}As (I = 3/2, 100%) nucleus with no $^{1}J(^{75}As–^{19}F)$ coupling being observed. Increasing the temperature to 20 °C, the doublet and quintets broadened to singlets with linewidth of approximately 350 and 450 Hz, respectively. Increasing the temperature somewhat slows down the rapid quadrupolar relaxation of ^{75}As, leading to introduction of collapsed $^{1}J(^{75}As-^{19}F)$ coupling, which manifests in significant broadening of the lines. Stronger bases than ketones, such as $N(CH_3)_3$, were shown to result in smaller electric field gradients about ^{75}As in the respective AsF_5 adduct [14]. As a consequence, equal-intensity quartet splitting of the resonances at −74.8 and −67.4 ppm had been observed in the ^{19}F NMR spectrum of $AsF_5{\cdot}N(CH_3)_3$ arising from $^{1}J(^{75}As–^{19}F)$ coupling of 840 and 1048 Hz, respectively. Doublet (67.4 ppm) and quintet (74.8 ppm) splittings arising from the $^{2}J(^{19}F–^{19}F)$ coupling of 120 Hz had also been discerned.

The observation of an additional resonance at −45.2 ppm ($\Delta\nu_{1/2}$ = 86 Hz) in the ^{19}F NMR spectrum (Fig. 2) alongside of that for $AsF_5{\cdot}O{=}C(CH_3)_2$ can be attributable to the $AsF_5{\cdot}OSO$ adduct, which formed due to a slight excess of AsF_5 in solution. This adduct was previously characterized by Raman spectroscopy and ^{19}F NMR spectroscopy [10,13]. The assignment was supported by the observation of a singlet at −44.7 ppm ($\Delta\nu_{1/2}$ = 88 Hz) in the ^{19}F NMR spectrum at −70 °C of a sample of AsF_5 in SO_2. Whereas the weakness of the dative bond in $AsF_5{\cdot}OSO$ allows for dissociation and chemical exchange of the fluorine environments, the stronger As---O interactions in the $AsF_5{\cdot}O{=}R$ adducts slows down the exchange between the fluorine environments, allowing for the observation of two environments and scalar $^{2}J(^{19}F–^{19}F)$ coupling. After warming the reaction to RT for 40 min, the ^{19}F resonance for $AsF_5{\cdot}OSO$ disappeared (Fig. S4), which is in line with the observed coloration of the solution at that temperature.

The ^{1}H and ^{13}C resonances of the ketones, acetone, cyclopentanone, and 2-adamantanone, are all shifted to higher frequencies upon addition of AsF_5 in SO_2 solvent (Table 3). Most notable is the significant deshielding of the ^{13}C resonance of the carbonyl carbon upon adduct formation ($AsF_5{\cdot}O{=}C(CH_3)_2$, $\Delta\delta(^{13}C)$ = 27.7 ppm; $AsF_5{\cdot}O{=}C_5H_8$, $\Delta\delta(^{13}C)$ = 27.0 Hz; $AsF_5{\cdot}O{=}C_{10}H_{14}$, $\Delta\delta(^{13}C)$ = 28.9 Hz). Such deshielding has previously been observed for Lewis-acid ketone adducts [5,7]. Interestingly, the α-carbons give rise to quintets in the ^{13}C NMR spectra of $AsF_5{\cdot}O{=}C(CH_3)_2$ and $AsF_5{\cdot}O{=}C_5H_8$, with couplings of 2.3 and 2.0 Hz, respectively. This coupling can be attributed to the $^{4}J(^{19}F_{eq}\text{-}^{13}C)$ coupling, which is not resolved in the ^{19}F NMR spectrum because of line broadening.

2.4. Computational Results

Density functional theory (DFT) calculations were carried out on the $AsF_5{\cdot}O{=}R$ adducts (R = $C(CH_3)_2$, C_5H_8, $C_{10}H_{14}$) along with their parent ketones using the B3LYP functional along with the aug-cc-pVTZ (used for $AsF_5{\cdot}O{=}C(CH_3)_2$) and cc-pVTZ (used for $AsF_5{\cdot}O{=}C_5H_8$ and $AsF_5{\cdot}O{=}C_{10}H_{14}$) basis sets. The gas-phase geometries of the compounds $AsF_5{\cdot}O{=}C(CH_3)_2$, $AsF_5{\cdot}O{=}C_5H_8$, and $AsF_5{\cdot}O{=}C_{10}H_{14}$, as well as the respective free ketones, were optimized and the geometric parameters can be found in Tables S4 - S6 (see Fig. 4). A summary of selected geometric parameters is given in Table 4. The adducts adopt a pseudo octahedral geometry around the As center and the As---O distances range between 2.044 ($AsF_5{\cdot}O{=}C_{10}H_{14}$) and 2.065 Å ($AsF_5{\cdot}O{=}C(CH_3)_2$). The shorter calculated As---O distance for adamantanone compared to acetone and cyclopentanone is in agreement with the largest decrease in C=O stretching frequency upon complexation with AsF_5 (vide supra). The ketones form Lewis acid-base interactions with AsF_5, which can be viewed as pnictogen bonding interactions. The As−O−C angles of 133.1, 130.3, and 132.6° for $AsF_5{\cdot}O{=}C(CH_3)_2$, $AsF_5{\cdot}O{=}C_5H_8$, and $AsF_5{\cdot}O{=}C_{10}H_{14}$, respectively are in

good agreement with those previously calculated for the $AsF_5 \cdot O{=}CF_2$, $AsF_5 \cdot O{=}CClF$, and $AsF_5 \cdot O{=}CCl_2$ adducts [5]. The As−O−C−C dihedral angles for each adduct deviate from 0 °C by no more than 1.9° ($AsF_5 \cdot O{=}C_5H_8$), resulting in the As−O−CC_2 moiety being essentially planar. These geometries were used to calculate the vibrational frequencies along with infrared and Raman intensities, which generally show excellent agreement with the experimental values (*vide supra*) (Tables S1 - S3).

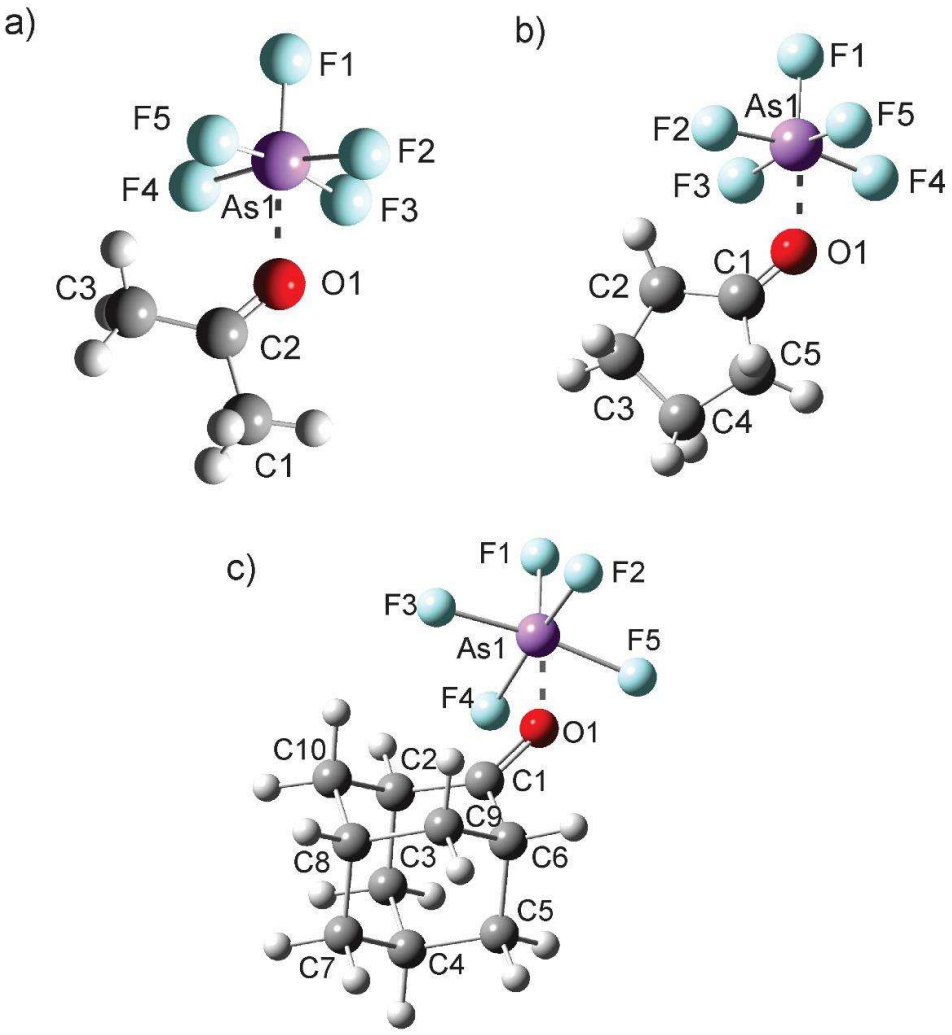

Fig. 4. Optimized gas-phase geometries of a) $AsF_5 \cdot O{=}C(CH_3)_2$, b) $AsF_5 \cdot O{=}C_5H_8$, and c) $AsF_5 \cdot O{=}C_{10}H_{14}$.

Table 4

Selected calculated bond lengths (Å) and bond angles (°) of $AsF_5{\cdot}O{=}C(CH_3)_2$, $AsF_5{\cdot}O{=}C_5H_8$, and $AsF_5{\cdot}O{=}C_{10}H_{14}$ adducts.

	C=O	$C_{C=O}{-}C^a$	$C_{C=O}{-}C^b$	O---As	As−O−C	As−O−C−C
$AsF_5{\cdot}O{=}C(CH_3)_2$ [c]	1.237	1.491	1.493	2.065	133.06	1.30
$O{=}C(CH_3)_2$ [c,e]	1.213	1.524	1.524	-	-	-
$AsF_5{\cdot}O{=}C_5H_8$ [d]	1.232	1.499	1.504	2.064	130.27	1.89
$O{=}C_5H_8$ [c,e]	1.205	1.528	1.528	-	-	-
$AsF_5{\cdot}O{=}C_{10}H_{14}$ [d]	1.240	1.497	1.501	2.044	132.56	0.00
$O{=}C_{10}H_{14}$ [c,e]	1.210	1.514	1.514	-	-	-

[a] Refers to the carbon *cis* to the As adducted to oxygen; [b] Refers to the carbon *trans* to the As adducted to oxygen; [c] DFT calculations at the B3LYP/aug-cc-pVTZ level of theory; [d] DFT calculations at the B3LYP/cc-pVTZ level of theory. [e] From reference 2.

Natural bond order (NBO) analyses were carried out to investigate the bonding in these $AsF_5{\cdot}O{=}R$ compounds (Tables S7 - S9). A summary of the NBO analyses is found in Table 5.

Table 5

Selected NPA charges, valences and Wiberg bond indices of the $AsF_5{\cdot}O{=}R$ (R = $C(CH_3)_2$, C_5H_8, and $C_{10}H_{14}$) compounds and their respective free ketones.

	NPA Charges (Valences [a])	NPA Charges (Valences [a])	Wiberg Bond Indices	
	O	C	CO	As---O
$O{=}C(CH_3)_2$	−0.55 (2.04)	0.59 (3.87)	1.83	
$AsF_5{\cdot}O{=}C(CH_3)_2$	−0.59 (2.14)	0.69 (3.78)	1.59	0.29
$O{=}C_5H_8$	−0.54 (2.06)	0.60 (3.87)	1.84	
$AsF_5{\cdot}O{=}C_5H_8$	−0.59 (2.15)	0.71 (3.77)	1.60	0.30
$O{=}C_{10}H_{14}$	−0.56 (2.04)	0.61 (3.87)	1.83	
$AsF_5{\cdot}O{=}C_{10}H_{14}$	−0.61 (2.14)	0.73 (3.76)	1.57	0.31

[a] Sum of the Wiberg Bond Indices per atom.

For each of the $AsF_5 \cdot O{=}R$ adducts, the Natural Population Analysis (NPA) charge on the carbonyl carbon increased by between 0.10 and 0.12, which is comparable to the monoprotonated ketones $[HO{=}R]^+$ ($R = C_{10}H_{14}, C_5H_8$, or $C(CH_3)_2$) studied where the charge on carbon increased by between 0.13 and 0.14 [2]. The negative charge on oxygen increased only by 0.04, for $AsF_5 \cdot O{=}C(CH_3)_2$, and 0.05, for $AsF_5 \cdot O{=}C_5H_8$, and $AsF_5 \cdot O{=}C_{10}H_{14}$, whereas a slight decrease in negative charge was observed for the $[HO{=}R]^+$ cations, resulting in a somewhat larger difference in NPA charges between C and O of the carbonyl group in the AsF_5 adduct (difference of 1.28 for $AsF_5 \cdot O{=}C(CH_3)_2$, versus 1.25 for $[HO{=}C(CH_3)_2]^+$). Looking at the calculated C=O Wiberg bond index (WBI), the $AsF_5 \cdot O{=}R$ adducts did not exhibit as great of a decrease in C=O bond order compared to the monoprotonated ketones. A decrease in WBI between 0.24 and 0.26 was calculated for $AsF_5 \cdot O{=}R$, whereas a decrease between 0.44 and 0.48 was calculated for the $[HO{=}R]^+$ cations, all relative to the free ketones. Hence, the oxonium resonance structure is dominant over the carbenium structure in the $AsF_5 \cdot O{=}R$ adducts (Scheme 1). The C=O bond in $AsF_5 \cdot O{=}R$ adducts is somewhat less polarized than in $[HO{=}R]^+$ cations, based on the lower bond index.

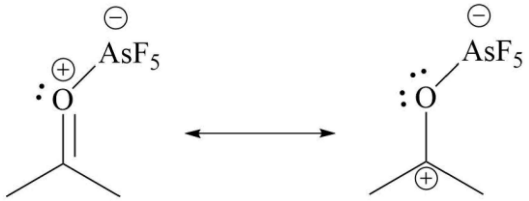

Oxonium Structure Oxocarbenium Structure

Scheme 1 Resonance structures for $AsF_5 \cdot O{=}C(CH_3)_2$.

The As---O bond index in the adducts range from 0.29 to 0.31, which is approximately half of that of the As–F bonds in the adducts (WBI = 0.56 to 0.62). For the protonated ketones, the

strong polarization of the C=O bond by protonation can be explained by the much higher O–H bond order (0.70) compared to that of the As---O bond.

The molecular orbital energies were calculated for the $AsF_5 \cdot O{=}R$ compounds (Fig. S5–S10). Using $AsF_5 \cdot O{=}C(CH_3)_2$ as a representative example, Fig. 5 shows the shapes and energies of the HOMO and LUMO upon addition of AsF_5. A dramatic decrease in energy by 771 kJ/mol is observed for the HOMO of $AsF_5 \cdot O{=}C(CH_3)_2$. The substantial decrease in energy of the HOMO significantly reduces the reactivity towards electrophilic attack. The HOMO also contains some π orbital contribution from the fluorine atoms of AsF_5 which might contribute to the considerable lowering in energy.

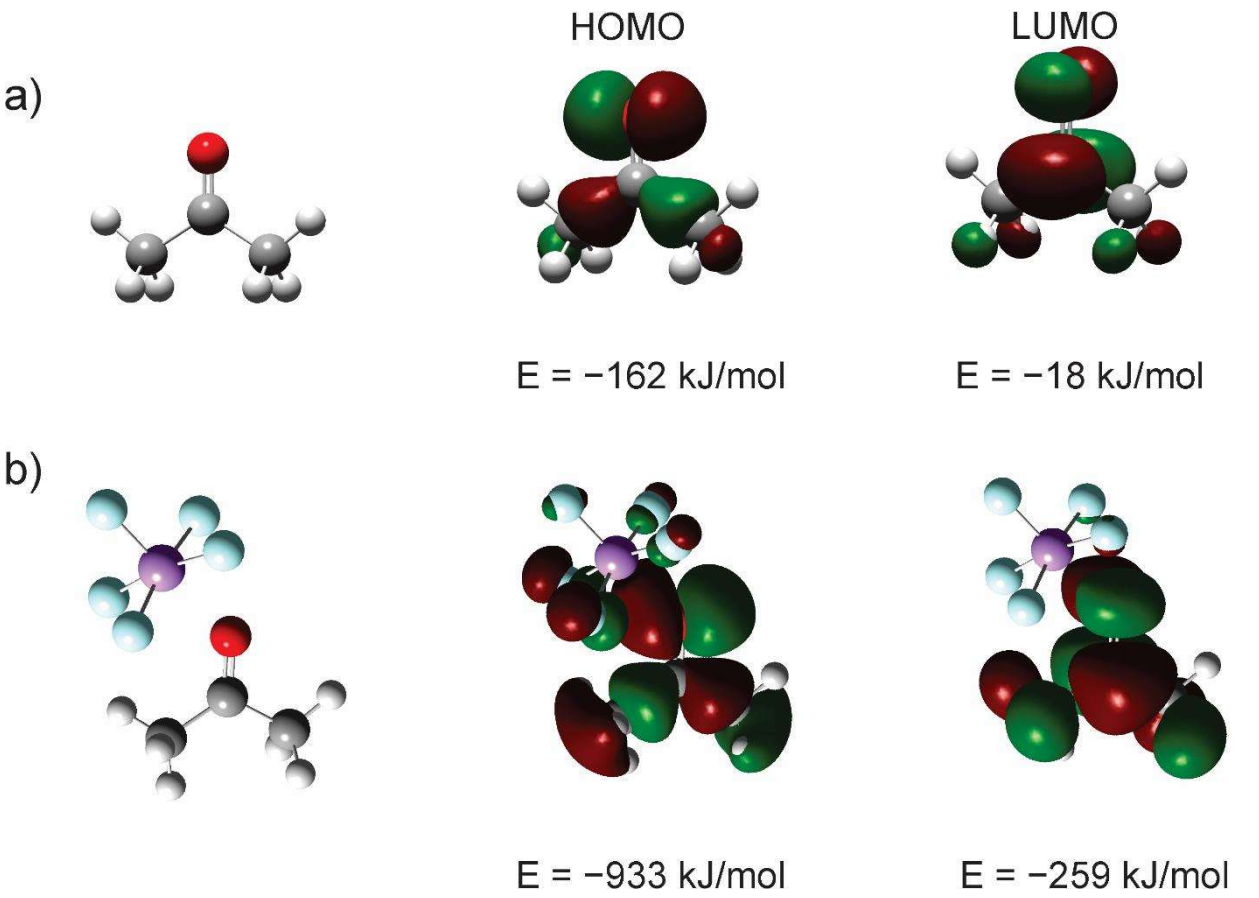

Fig. 5. Molecular orbitals of a) acetone and b) $AsF_5 \cdot O{=}C(CH_3)_2$. From left to right are the reference molecules, HOMO diagrams, and LUMO diagrams.

More interestingly, the formation of the C=O---As moiety also dramatically lowers the LUMO by 241 kJ/mol of acetone, creating a species that is much more reactive towards nucleophilic attack compared to the free ketone. A summary of the HOMO and LUMO energies for the $AsF_5{\cdot}O{=}R$ adducts and $[HO{=}R]^+$ cations is given in Table 6. Surprisingly, the LUMO energy of $AsF_5{\cdot}O{=}C(CH_3)_2$ (−259 kJ/mol) is substantially lower than that of $[HO{=}C(CH_3)_2]^+$ (−189 kJ/mol). While the partial charge on the carbon of the C=O bond is larger in the protonated ketones, the LUMO energies of the AsF_5 ketone adducts are lower, indicating a higher electrophilicity of the Lewis acid adducts of ketones compared to the protonated ketones. A previous study investigating the change in energy of the HOMO and LUMO of $BF_3{\cdot}$acetaldehyde only showed a decrease of 80 kJ/mol in the LUMO and 173 kJ/mol in the HOMO [3]. This smaller energy change can be attributed to the weaker Lewis acidity of BF_3 compared to AsF_5, whereby the C=O---As moiety more heavily influences the reactivity of the ketone.

Table 6

Calculated energies (kJ/mol) of the HOMO and LUMO for the $AsF_5{\cdot}O{=}R$ adducts and the protonated ketones $[H(O{=}R)_x]^+$ (x = 1 or 2; R = $C(CH_3)_2$, C_5H_8, $C_{10}H_{14}$).

Compound	HOMO Energy	LUMO Energy
$O{=}C_{10}H_{14}$	−151	−13
$[HO{=}C_{10}H_{14}]^+$	−286	−163
$AsF_5{\cdot}O{=}C_{10}H_{14}$	−837	−229
$O{=}C_5H_8$	−157	−20
$[HO{=}C_5H_8]^+$	−323	−182
$AsF_5{\cdot}O{=}C_5H_8$	−890	−256
$O{=}C(CH_3)_2$	−162	−18
$[HO{=}C(CH_3)_2]^+$	−376	−189
$[H(O{=}C(CH_3)_2)_2]^+$	−1203	−596
$AsF_5{\cdot}O{=}C(CH_3)_2$	−933	−259

3. Conclusions

For the first time, Lewis acid-base adducts of aliphatic and alicyclic ketones with AsF_5 were synthesized and characterized by Raman, ^{1}H, ^{13}C, and ^{19}F NMR spectroscopies. These $AsF_5{\cdot}O{=}R$ adducts (R = $C(CH_3)_2$, C_5H_8, $C_{10}H_{14}$) were isolated as white powders and found to slowly and, in the case of $AsF_5{\cdot}O{=}C(CH_3)_2$, rapidly decompose at RT. Raman spectroscopy showed characteristic bands of the ketones that are shifted upon addition of AsF_5 and subsequent adduct formation. Specifically, the C=O stretching frequency dramatically decreased by between 107−151 cm^{-1} and ν(CCC) stretches and ring breathing modes of the ketones shift to higher frequencies. The ^{19}F NMR spectra of these compounds showed they had developed pseudo octahedral geometries about the ^{75}As metal center. While no $^{1}J(^{75}As{-}^{19}F)$ coupling was observed, the $^{2}J(^{19}F{-}^{19}F)$ coupling between the axial and equatorial fluorine environments of AsF_5 appeared in the ^{19}F NMR spectra. Long-range $^{4}J(^{19}F\text{-}^{13}C)$ coupling between the equatorial fluorines on the AsF_5 moiety and the α-carbon were observed for $AsF_5{\cdot}O{=}C(CH_3)_2$ and $AsF_5{\cdot}O{=}C_5H_8$.

NBO analyses of these $AsF_5{\cdot}O{=}R$ adducts showed an increase in the charge of the carbon of the carbonyl group and a decrease in the C=O bond order due to the strong Lewis acid, AsF_5, withdrawing electron density from the C=O group. Decreases in the HOMO and LUMO energies also confirmed the activation and increased reactivity of the ketones in Lewis-acid catalyzed organic reactions. These results are comparable to the oxonium $[HO{=}R]^{+}$ cations (R = $C(CH_3)_2$, C_5H_8, $C_{10}H_{14}$) typically observed as intermediates in Brønsted acid-catalyzed organic reactions. DFT calculations predicted the C=O bond of $AsF_5{\cdot}O{=}R$ adducts to contain less single-bond character than the $[HO{=}R]^{+}$ cations. While the partial charge of the carbonyl carbon is increased to a lesser extent by AsF_5 compared to protonation, it is interesting that the LUMO of the

$AsF_5 \cdot O{=}R$ adduct is substantially lower in energy than the $[HO{=}R]^+$ cation reflecting the reactivity of adducts of carbonyl compounds with Lewis acids.

4. Experimental

4.1. General procedures and materials

Caution: Arsenic pentafluoride is highly toxic and produces HF upon contact with moisture, which can cause severe burns upon contact or inhalation. Therefore, AsF_5 should be manipulated under rigorously dry conditions and appropriate safety measures should be implemented during handling.

All reactions were carried out in heat-sealed ¼"-o.d. or 4-mm o.d. FEP reactors which were connected to either stainless-steel or Kel-F valves via flared fittings. Volatile materials were distilled on a Pyrex vacuum line equipped with glass valves fitted with 6-mm-o.d. PTFE J. Young stopcocks, with the exceptions of AsF_5, which was distilled through a metal vacuum line equipped with 316 stainless-steel valves (Autoclave Engineers) and pre-passivated with 100% F_2. Solid materials were handled in a dry box (Omni Lab, Vacuum Atmospheres) under an atmosphere of dry N_2.

Sulfur dioxide (Matheson) was dried over CaH_2. Dichloromethane was distilled from a solvent system onto 4-Å molecular sieves and then distilled onto fresh sieves. Arsenic pentafluoride, AsF_5, was prepared according to the literature procedure and stored in a nickel reactor with a monel (Autoclave Engineers) valve [15]. AsF_3 was dried over NaF for 24 h to remove any trace amounts of HF which was subsequently transferred to a ¾-in. o.d. FEP reactor and directly fluorinated with an excess of F_2 to yield hydrogen fluoride-free AsF_5.

4.2. Synthesis of $AsF_5 \cdot O{=}C(CH_3)_2$

On a metal vacuum line, AsF_5 (0.046 g, 0.27 mmol) was distilled into a 4-mm FEP reactor at −196 °C. The reactor was connected to a glass vacuum line where an excess of SO_2 (ca. 0.4 mL) was distilled onto the AsF_5 and dissolved at −60 °C to give a clear, colourless solution. Slightly less than one molar equivalent of acetone (0.020 g, 0.24 mmol) was distilled into a glass graduated weighing vessel equipped with a J. Young PTFE stopcock and, subsequently, distilled onto the AsF_5/SO_2 solution at −196 °C. A clear, colourless solution resulted upon warming the reactor to −70 °C. The reactor was heat sealed under dynamic vacuum and the contents of the reaction were characterized using ^{19}F, ^{13}C and ^{1}H NMR spectroscopy at −70 °C. Small amounts of $[HO{=}C(CH_3)_2][AsF_6]$ were detected presumably because of a small concentration of HF in the sample.

Using the same method, the reaction was also carried out in a ¼-in. o.d. FEP reactor. AsF_5 (0.066 g, 0.39 mmol) was dissolved in SO_2 and acetone (0.025 g, 0.43 mmol) was distilled onto the mixture. The reaction was warmed to −70 °C and a fine, white powder-like suspension crashed out of solution. The solid was dissolved upon agitation and, upon slowly cooling, the white powder reappeared. Crystal growth was attempted by slowly cooling the sample, as well as, slowly removing the SO_2 at −70 °C; however, no evidence for crystal formation appeared. The white solid was characterized by Raman spectroscopy at −100 °C.

4.3. Synthesis of $AsF_5{\cdot}O{=}C_5H_8$

Cyclopentanone (0.013 g, 0.15 mmol) was distilled into the 4-mm reactor. An excess of CH_2Cl_2 (ca. 0.5 mL) was distilled onto the cyclopentanone yielding a clear, colourless solution at RT. Approximately one molar equivalent of AsF_5 (0.15 mmol) was distilled through a metal vacuum line into the reactor containing cyclopentanone and CH_2Cl_2 at −196 °C. Upon warming the reaction to −79 °C, a fine white powder was suspended in solution. All volatiles were pumped

off at −70 °C yielding a white powder, which was characterized by Raman spectroscopy at −100 °C and shown to be $AsF_5 \cdot O{=}C_5H_8$. An excess of SO_2 was distilled onto the $AsF_5 \cdot O{=}C_5H_8$ adduct and dissolved at −50 °C. The reactor was heat sealed under dynamic vacuum and the $AsF_5 \cdot O{=}C_5H_8$ adduct was further characterized using ^{19}F, ^{13}C and ^{1}H NMR spectroscopy at −70 °C. Small amounts of $[HO{=}C_5H_8][AsF_6]$ were detected presumably because of a small concentration of HF in the sample.

4.4. Synthesis of $AsF_5 \cdot O{=}C_{10}H_{14}$

2-Adamantanone (0.016 g, 0.11 mmol) was loaded into a 4-mm FEP reactor inside a nitrogen-atmosphere dry box followed by distillation of ca. 0.3 mL of SO_2 yielding a solution at RT. One molar equivalent of AsF_5 (0.11 mmol) was distilled through a metal vacuum line into the reactor at −196 °C. A clear, colourless solution was obtained upon warming the reactor to −70 °C. The reactor was heat sealed under dynamic vacuum and the product was characterized using ^{19}F, ^{13}C and ^{1}H NMR spectroscopy at −70 °C and found to be the $AsF_5 \cdot O{=}C_{10}H_{14}$ adduct.

Using a similar method, the reaction was also carried out in a ¼-in. o.d. FEP reactor. 2-Adamantanone (0.019 g, 0.13 mmol) was dissolved in CH_2Cl_2 (ca. 0.6 mL) at RT and approximately one equivalent of AsF_5 (0.15 mmol) was distilled onto the mixture. The reaction was warmed to −80 °C giving a clear, light yellow solution. The CH_2Cl_2 was pumped off at −70 °C into a glass U-trap at −196 °C until a white powder remained. This was characterized by Raman spectroscopy at −100 °C and shown to be $AsF_5 \cdot O{=}C_{10}H_{14}$. Crystal growth was attempted, however, no evidence for crystal formation appeared.

4.5. Raman Spectroscopy

All Raman spectra were recorded on solid samples in FEP tubes using a Bruker RFS-100 Raman spectrometer outfitted with a quartz beam-splitter and liquid-N_2-cooled germanium

detector. The 1064-nm line of a Nd:YAG laser was used for excitation of the sample, and back-scattered (180°) radiation was sampled. The usable Stokes range of the collected data was 85 to 3500 cm^{-1} with a resolution of 2 cm^{-1}. The laser power was typically set to 150 mW.

4.6. NMR Spectroscopy

All NMR spectra were recorded in heat-sealed 4-mm o.d. FEP tubes inserted into 5-mm o.d. glass NMR tubes using a Bruker Avance II 300 MHz spectrometer equipped with a 5-mm broadband probe. Spectra were recorded unlocked, and referenced externally to $CFCl_3$ (^{19}F) and $Si(CH_3)_4$ (^{1}H, ^{13}C) at 20 °C. Spectral simulations were performed using Mestre Nova [16].

4.7. Computational Details

All DFT calculations were performed at the B3LYP/aug-cc-pVTZ ($AsF_5{\cdot}O{=}C(CH_3)_2$,) and B3LYP/cc-pVTZ ($AsF_5{\cdot}O{=}C_5H_8$, and $AsF_5{\cdot}O{=}C_{10}H_{14}$) levels of theory since these techniques provide reliable structural information. Energy-minimized geometries were used to calculate B3LYP/aug-cc-pVTZ vibrational frequencies along with the IR and Raman intensities. No scaling factors were used on the calculated vibrational frequencies. Calculations were performed using Gaussian 09 (revision D.01) [17], and the NBO program (version 6.0) was used for the NBO analyses [18]. The GaussView visualization software was used to visualize the vibrational displacements and aid in assignments of the bands, and visualize molecular orbitals [19].

Acknowledgements

We would like to thank the Natural Sciences and Engineering Research Council of Canada (M.G. and S.D.W.: Discovery grants) and the University of Lethbridge for supporting this work. Computational studies were performed using equipment funded through the Canada Foundation of Innovation, as well as resources made available through Westgrid and Compute/Calcul Canada. We thank Douglas Turnbull for his help with acquiring NMR spectra.

References

[1] W. R.. Hasek, W. C. Smith, V. A. Engelhardt, The Chemistry of Sulfur Tetrafluoride. II. The Fluorination of Organic Carbonyl Compounds, J. Am. Chem. Soc. 62 (1960) 543-551.

[2] D. Stuart, S. D. Wetmore, M. Gerken, Solid-State Structure of Protonated Ketones and Aldehydes, Angew. Chem. Int. Ed. 56 (2017) 16380–16384.

[3] M. T. Reetz, M. Hüllmann, W. Massa, S. Berger, P. Rademacher, P. Heymanns, Structure and Electronic Nature of the Benzaldehyde/Boron Trifluoride Adduct, J. Am. Chem. Soc. 108 (1986) 2405–2408.

[4] K. O. Christe, The Interaction of Phosgene with Lewis Acids, Inorg. Chem. 6 (1967) 1706–1710.

[5] H. Berthold, J. A. Boatz, J. Hegge, K. O. Christe, Experimental and Theoretical Characterization of the Oxygen-Coordinated Donor-Acceptor Adducts of $COCl_2$, COClF, and COF_2 with AsF_5 and SbF_5, Inorg. Chem. 38 (1999) 3143–3149.

[6] S. Shambayati, S. L. Schreiber, Lewis Acid Carbonyl Complexation, In *Comprehensive Organic Synthesis*; Trost, B. M.; Fleming, I., Eds.; Pergamon: Oxford, 1991; Vol. *1*, 283–324.

[7] (a) T. Laube, H. U. Stilz, Crystal Stucture of the Complex 5-Phenyladamantan-2-one-Pentachloroantimony. Hyperconjugative Effects in an Activated Ketone, Am. Chem. Soc. 109 (1987) 5876-5878; (b) T. Laube, A. Weidenhaupt, R. Hunziker, Activation of α-Bromo Ketones by Complexation with Hard and Soft Lewis Acids. A Combined X-ray and NMR Study, J. Am. Chem. Soc. 113 (1991) 2561-2567; (c) T. Laube, S. Hollenstein, Crystal Structures of Two Activated Cyclohexanones with Opposite Pyramidalizations of the Carbonyl Groups, J. Am. Chem. Soc. 114 (1992) 8812-8817.

[8] J. S. Hartman, P. Stilbs, S. Forsén, An NMR Study of Conformational Exchange in some Ketone-BF_3 and Ether-BF_3 Adducts, Tetrahedron Lett. 40 (1975) 3497–3500.

[9] A. Bittner, D. Männig, H. Nöth, Solutions of Aluminium Trichloride in Tetramethylurea and the Molecular Structure of an Aluminium Trichloride Tetramethylurea Adduct, Z. Naturforsch., 41b (1986) 587–591.

[10] G. S. H. Chen, J. Passmore, Identification by Raman Spectroscopy of Various Weak Oxygen-bridged Donor-Acceptor Adducts of Arsenic and Antimony Pentafluorides; a Reversal of the Usual Lewis Acidities of these Pentafluorides towards Sulphuryl Fluoride, J. Chem. Soc. Dalton Trans. (1979) 1257–1261.

[11] K. O. Christe, B. Hoge, J. A. Boatz, G. K. S. Prakash, G. A. Olah, J. A. Sheehy, Existence of the Halocarbonyl and Trifluoromethul Cations in the Condensed Phase, Inorg. Chem. 38 (1999) 3132-3142.

[12] H. Vančik, V. Gabelica, Z. Mihalić, D. E. Sunko, Complexes of Ketones with SbF_5 in the Condensed Phase. Structural Effects on the Carbonyl Stretching Frequencies, J. Chem. Soc. Perkin Trans II (1992) 1611–1614.

[13] M. Brownstein, R. J. Gillespie, Nuclear Magnetic Resonance Investigation of Complexes Formed by Arsenic Pentafluoride and Some Very Weak Bases, J. Am. Chem. Soc. 92 (1970) 2718−2721.

[14] L. Lunazzi, S. Brownstein, Proton and Fluorine Resonance Spectra of Some Complexes of PF_5 and AsF_5, J.Magn. Reson. 1 (1969) 119−123.

[15] A. A. A. Emara, J. F. Lehmann, G. J. Schrobilgen, A laboratory-scale synthesis of high-purity AsF_5 by direct fluorination of AsF_3, J. Fluorine Chem. 126 (2005) 1373-1376.

[16] MestRe Nova, version 9.0; Mestrelab Research S.L.; Santiago de Compostela, Spain (2014).

[17] Frisch, M. J.; Trucks, G. W.; Schlegel, H. B.; Scuseria, G. E.; Robb, M. A.; Cheeseman, J.R.; Scalmani, G.; Barone, V.; Petersson, G. A.; Nakatsuji, H.; et al. Gaussian 09, Revision D.01; Gaussian, Inc: Wallingford, CT, 2016.

[18] Glendening, E. D.; Badenhoop, J. K.; Reed, A. E.; Carpenter, J. E.; Bohmann, J. A.; Morales, C. M.; Landis, C. R.; Weinhold, F. NBO 6.0. Theoretical Chemistry Institute, University of Wisconsin: Madison, WI, 2013.

[19] GaussView, version 3.0; Gaussian Inc.: Pittsburgh, PA, 2003.